25. D. G. Myszka *et al.*, *Proc. Natl. Acad. Sci. U.S.A.* **97**, 9026 (2000).
26. P. D. Kwong *et al.*, *Structure Fold. Des.* **8**, 1329 (2000).
27. G. M. Morris *et al.*, *J. Comp. Chem.* **19**, 1639 (1998).
28. AutoDock 3.0.5 was used to perform all protein-protein docking experiments by using the Lamarckian Genetic Algorithm (*27*). AutoGrid chemical affinity and electrostatics maps were computed and centered on gp120 with 126 × 126 × 126 grid points at a spacing of 1 Å. As a test of the method, AutoDock was able to dock the D1 domain of CD4 onto gp120 to recreate the crystallized complex of CD4 and gp120 to within 0.5 Å root mean square (rms) deviation. For CD4-gp120 docking, correct solutions clustered together at about −21 kcal/mol, whereas the next lowest energy solutions were about −11 kcal/mol. In order to reduce the number of atoms in the large b12-gp120 docking experiment, we docked only the Fv domain instead of the intact IgG. The two lowest energy dockings could be ruled out because the antibody constant domains overlapped gp120 when the full antibody was reconstructed from the Fv fragment. The next four lowest energy dockings formed the largest cluster, and had a median rms deviation of 2.3 Å from the initial model generated by hand from geometric constraints. This initial model complex was solvated by a 5 Å shell of water molecules, and energy minimization performed by using the Discover 3 module of Insight II 2000 package (Molecular Simulations, San Diego, CA) and the CVFF force field for 100 iterations. This short minimization was enough to relieve any close contacts. Docking of the minimized structures resulted in a large 11-member cluster of solutions, with an average energy of −24.7 kcal/mol, unambiguously separated in energy from the remaining solutions.
29. P. Roben *et al.*, *J. Virol.* **68**, 4821 (1994).
30. J. P. Moore, J. Sodroski, *J. Virol.* **70**, 1863 (1996).
31. W. P. Yang *et al.*, *J. Mol. Biol.* **254**, 392 (1995).
32. M. B. Zwick *et al.*, unpublished data.
33. J. M. Binley *et al.*, *AIDS Res. Hum. Retrovir.* **14**, 191 (1998).
34. H. R. Gelderblom, E. H. Hausmann, M. Ozel, G. Pauli, M. A. Koch, *Virology* **156**, 171 (1987).
35. D. R. Burton, E. O. Saphire, P. W. H. I. Parren, *Curr. Top. Microbiol. Immunol.* **260**, 109 (2001).
36. I. Sanz, *J. Immunol.* **147**, 1720 (1991).
37. P. E. Dawson, T. W. Muir, I. Clark-Lewis, S. B. Kent, *Science* **266**, 776 (1994).
38. Z. Otwinowski, W. Minor, *Methods Enzymol.* **276**, 307 (1997).
39. J. Navaza, *Acta Crystallogr.* **A50**, 157 (1994).
40. A. T. Brünger *et al.*, *Acta Crystallogr.* **D54**, 905 (1998).
41. T. A. Jones, in *Computational Crystallography*, D. Sayre, Ed. (Oxford Univ. Press, Oxford, 1982), pp. 303–317.
42. K. D. Cowtan, P. Main, *Acta Crystallogr.* **D52**, 43 (1996).
43. R. A. Laskowski, M. W. MacArthur, D. S. Moss, J. M. Thornton, *J. Appl. Crystallogr.* **26**, 283 (1993).
44. R. M. Esnouf, *Acta Crystallogr.* **D55**, 938 (1999).
45. E. A. Merritt, D. J. Bacon, *Methods Enzymol.* **277**, 505 (1997).
46. Supplementary material is available in *Science* Online at www.sciencemag.org/cgi/content/full/293/5532/1155/DC1.
47. E.O.S., M.B.Z., A. Menendez, P.W.H.I.P., D.R.B., J. K. Scott, and I.A.W., unpublished observations.
48. M. F. Sanner, A. J. Olson, J. C. Spehner, *Biopolymers* **38**, 305 (1996).
49. M. F. Sanner, *J. Mol. Graph. Mod.* **17**, 57 (1999).
50. H. Mo *et al.*, *J. Virol.* **71**, 6869 (1997).
51. P. Poignard *et al.*, *Immunity* **10**, 431 (1999).
52. Supported by NIH Grants GM46192 (I.A.W.), AI40377 (P.W.H.I.P.), and AI33292 (D.R.B.). We are extremely grateful to the staff of the Stanford Synchrotron Radiation Laboratory (SSRL) Beamline 7-1 for assistance in data collection, M. Wormald of the Oxford Glycobiology Institute (UK) for discussions of carbohydrate torsion angles, A. de Vos of Genentech for human Fc coordinates, J. Sodroski of Harvard University for plasmid pSVIIIenv, V. Roberts for discussions of electrostatics and docking, P. Dawson for peptide synthesis, P. Poignard for help with gp120 mutagenesis, and M. Wang and A. Hessell for technical assistance. This is publication 13874-MB from The Scripps Research Institute. The IgG1 b12 coordinates and structure factors have been deposited into the Protein Data-bank (PDB accession code 1HZH) and are available from wilson@scripps.edu.

17 April 2001; accepted 18 June 2001

Enforcement of Temporal Fidelity in Pyramidal Cells by Somatic Feed-Forward Inhibition

Frédéric Pouille and Massimo Scanziani*

The temporal resolution of neuronal integration depends on the time window within which excitatory inputs summate to reach the threshold for spike generation. Here, we show that in rat hippocampal pyramidal cells this window is very narrow (less than 2 milliseconds). This narrowness results from the short delay with which disynaptic feed-forward inhibition follows monosynaptic excitation. Simultaneous somatic and dendritic recordings indicate that feed-forward inhibition is much stronger in the soma than in the dendrites, resulting in a broader integration window in the latter compartment. Thus, the subcellular partitioning of feed-forward inhibition enforces precise coincidence detection in the soma, while allowing dendrites to sum incoming activity over broader time windows.

At certain brain synapses, reliable transmission is ensured through large, rapidly rising, excitatory postsynaptic potentials (EPSPs), which are able to trigger a spike with little latency variation (*1*).

In hippocampal pyramidal cells (PCs), the small size of most unitary EPSPs requires that synaptic activity summate to reach the spike threshold (*2*). In principle, the relatively long membrane time constant of these neurons (*3*) may allow EPSPs to summate over large time windows. The occurrence of spikes would then reflect the average synaptic bombardment over time instead of being selectively time-locked to coincident synaptic activity. Thus, it is not known whether the timing of a spike in PCs reports the timing of the afferent activity triggering the spike (*4–6*). This issue can be addressed experimentally by determining the time window within which the activity of independent synaptic inputs must occur to trigger a spike.

We recorded from CA1 PCs in acute hippocampal slices from rat brains in cell-attached mode to avoid interfering with the intracellular ionic composition. Two stimulation electrodes were placed in the stratum radiatum at 300 to 600 μm on each side of the recorded neuron (*7*). Stimulation intensity was set so that when the two Schaffer collateral pathways were stimulated simultaneously, the PC fired a spike, detected as a capacitive current, in about 50% of the trials (threshold stimulation). The probability of spiking steeply decreased when one of the stimuli was shifted in time in 2.5- or 5-ms steps (Fig. 1A). A Gaussian fit of the data gave a SD of 1.4 ms ($n = 9$ cells).

We then blocked γ-aminobutyric acid A receptors ($GABA_A R$) with bicuculline (20 μM) or with the more selective antagonist SR95531 (3 μM) (*8*) and readjusted the stimulation intensity of both pathways to match the spiking probability observed under control conditions with simultaneous stimulation ($51 \pm 3\%$ in control conditions versus $50 \pm 5\%$ in the presence of bicuculline, $n = 5$ cells; $62 \pm 6\%$ in control conditions versus $64 \pm 11\%$ in the presence of SR95531, $n = 4$ cells). This increased the delay between stimulus and spike (8.2 ± 0.6 ms in control conditions, 16.8 ± 1.2 ms in the presence of $GABA_A R$ antagonist; $n = 9$ cells).

$GABA_A R$ antagonists greatly prolonged the integration window (SD = 17.8 ms in bicuculline, $n = 5$ cells; SD = 15.6 ms in SR95531, $n = 4$ cells). In addition, although spikes triggered with simultaneous stimulation under control conditions showed submillisecond variability in spike delay (jitter), as described for intracellular current injections (*9*), in the presence of $GABA_A R$ antagonists the jitter increased almost threefold (the SD was 0.5 ms in control conditions versus 1.4 ms with $GABA_A R$ antagonists, $n = 9$ cells; Fig. 1B).

We monitored the underlying synaptic events using whole-cell recordings. In voltage-clamped cells, a stimulus elicited an excitatory postsynaptic current (EPSC)–inhibi-

Brain Research Institute, University of Zurich, Winterthurerstrasse 190, CH-8057 Zurich, Switzerland.

*To whom correspondence should be addressed. E-mail: massimo@hifo.unizh.ch

tory postsynaptic current (IPSC) sequence. The IPSC, which could be blocked by bicuculline, had a delayed onset with respect to the EPSC (1.9 ± 0.2 ms, $n = 9$ cells; Fig. 2A). Under current-clamp conditions, a stimulus elicited an EPSP-IPSP sequence (10), which was strongly reduced by bath perfusion of the α-amino-3-hydroxyl-5-methyl-4-isoxazole-propionate (AMPA)/kainate receptor antagonist NBQX [20 to 40 μM; EPSP, $114 \pm 5\%$ reduction; IPSP, $91 \pm 2\%$ reduction (11); $n = 12$ (six cells, 12 pathways); Fig. 2A], indicating that the stimulation of Schaffer collaterals leads to synaptic activation of GABAergic interneurons (feed-forward inhibition).

This was not due to the stimulation of large numbers of Schaffer collaterals, because even the weakest stimulation intensities, still producing a detectable postsynaptic response, evoked a delayed inhibitory component (2.9 ± 1 nS; $n = 14$ cells; Fig. 2B) (12). In addition, brief puffs of potassium solution focally applied onto the CA3 PC layer evoked clear EPSC-IPSC sequences in CA1 PCs ($n = 5$ cells; Fig. 2C) (13).

These results are consistent with previous observations indicating that spikes in interneurons can be triggered by unitary EPSPs (14–16) and suggest that CA3 to CA1 signaling occurs via a canonical EPSP-IPSP sequence (Fig. 2D).

To determine the integration window in current-clamp conditions, we set the stimulation intensity at the threshold for spike generation when two pathways were stimulated simultaneously and readjusted the intensity to keep spiking probability constant after the perfusion of GABA$_A$R antagonists ($58 \pm 5\%$ in control conditions, $56 \pm 2\%$ in GABA$_A$R antagonists; $n = 8$ cells (five in bicuculline, three in SR95531) (17). This decreased the initial slope of the EPSP by $80 \pm 4\%$ [$n = 6$ (three cells in SR95531, six pathways)], indicating that without feed-forward inhibition, a fifth of the excitatory fibers originally recruited are sufficient to reach threshold. The slower depolarization is likely to underlie the increased spike delay (6.9 ± 0.5 ms versus 16.1 ± 0.8 ms; $n = 8$ cells) and jitter (0.6 ms versus 1.8 ms; $n = 8$ cells; Fig. 2F) (18). The integration window increased from 1.6 ms in control conditions to 14.8 ms with GABA$_A$R antagonists ($n = 8$ cells; Fig. 2E).

Different classes of GABAergic interneurons selectively innervate different subcellular compartments of PCs (19). To reveal the subcellular target of feed-forward inhibition on CA1 PCs, we simultaneously recorded from the soma and apical dendrite (20). The Schaffer collateral-evoked EPSP recorded in the dendrites was larger by $368 \pm 112\%$ [4.2 ± 0.5 mV in the dendrite

versus 1.2 ± 0.3 mV in the soma; $n = 10$ (nine cells, 10 pathways; the average distance between pipettes was 211 ± 19 μm, and the range was from 120 to 341 μm)] and had a steeper initial slope compared with the somatic response [1.5 ± 0.2 mV/ms versus 0.6 ± 0.1 mV/ms, $P < 0.01$; $n = 10$ (nine cells, 10 pathways); Fig. 3A]. In bicuculline, EPSPs recorded in the dendrite were only $15 \pm 5\%$ larger than those recorded in the soma [6.2 ± 0.7 mV versus 5.5 ± 0.6 mV in the soma; $n = 10$ (nine cells, 10 pathways)] and EPSP half-decay times did not significantly differ between compartments [38.6 ± 6.9 ms versus 40.9 ± 6.2 ms; $P > 0.28$; $n = 10$ (nine

cells, 10 pathways); Fig. 3, A and B]. In bicuculline, initial slopes remained unchanged, confirming the lack of direct activation of inhibitory fibers [0.6 ± 0.1 mV/ms in control versus 0.7 ± 0.1 mV/ms in bicuculline (measured in the soma); $P > 0.26$; $n = 10$ (nine cells, 10 pathways); Fig. 3B]. The bicuculline-sensitive area (21) was significantly greater in the soma by $24 \pm 5\%$ ($P < 0.001$; $n = 9$ cells; Fig. 3B) (22). In addition, the bicuculline-sensitive area in dendritic recordings decreased with increasing distance from the soma (Fig. 3B). To test whether an exclusively somatic inhibition could account for the above observation, we imposed an inhibitory con-
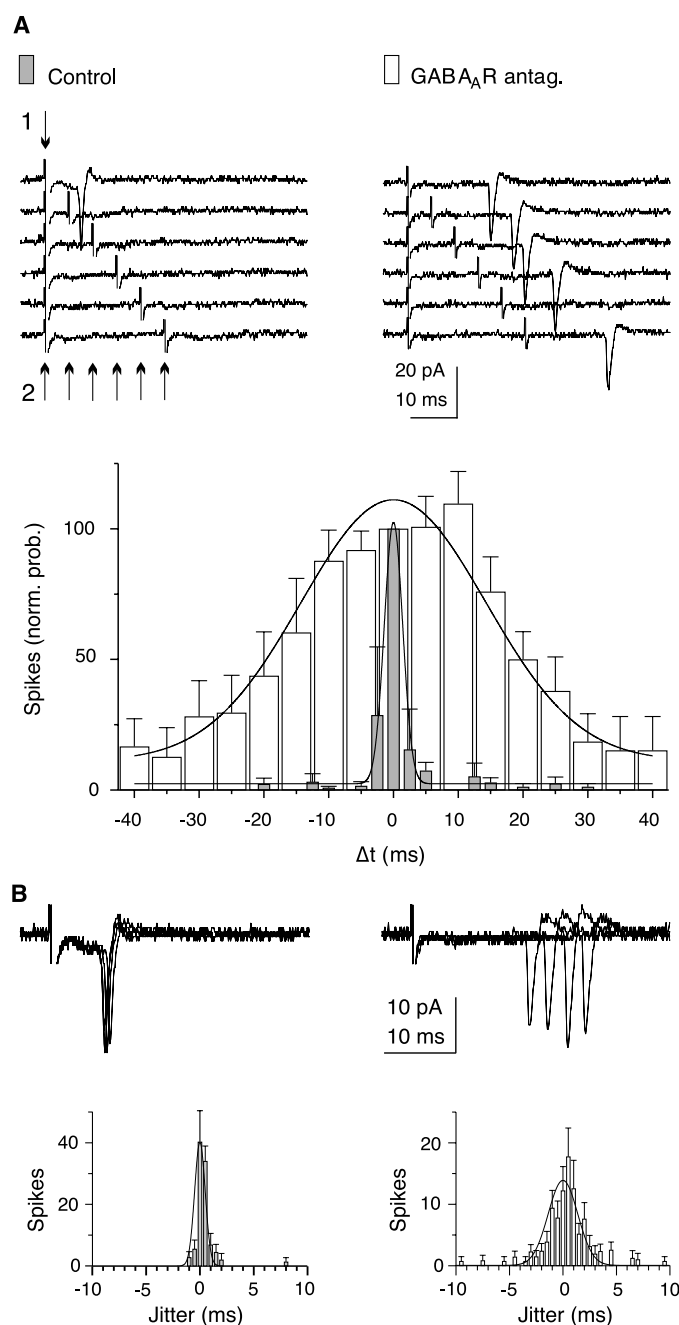

Fig. 1. Coincidence detection in PCs is abolished by GABA$_A$R antagonists. (**A**) Current traces showing cell-attached recordings from CA1 PCs upon stimulation of two Shaffer collateral pathways. Each sweep shows a different interstimulus interval (ISI) between pathways. (Upper left) In control conditions, a spike is triggered only upon simultaneous stimulation of pathways 1 and 2. (Upper right) In bicuculline, spikes are also triggered with larger ISIs. (Bottom) Histogram showing normalized probability of spike generation plotted against ISIs ($n = 9$ cells). The solid columns show control conditions (bin width, 2.5 ms for ISIs between ± 15 ms and 5 ms for longer ISIs). The open columns show conditions in GABA$_A$R antagonists (bin width, 5 ms). Norm. prob., normalized probability; Δt, interstimulus interval. (**B**) Same cell as in (A). (Upper panels) Current traces; four superimposed sweeps were recorded upon simultaneous stimulation of both pathways without (left) and with (right) bicuculline. (Bottom) Histograms showing the probability distribution of the time of spike occurrence ($n = 9$ cells; bin width, 500 μs).

ductance (dynamic clamp) through the somatic pipette 2 ms after the onset of Schaffer collateral-evoked EPSPs in the presence of the GABA$_A$R antagonist SR95531 (3 μM; the average distance between pipettes was 200 ± 14 μm, and the range was from 143 to 255 μm; $n = 9$ cells; Fig. 3C) (23). The attenuation of the simulated IPSP-sensitive area was not significantly different from the decrease in the bicuculline-sensitive area ($P > 0.26$; Fig. 3D) (24).

We compared the time window of EPSP summation between the soma and the dendrites of CA1 PCs (the average distance between pipettes was 229 ± 30 μm, and the range was from 120 to 323 μm; $n = 6$ cells; Fig. 4A). The graph illustrates that although the soma effectively summates EPSPs over a time window ranging from –1.5 to +2.4 ms, effective summation of EPSPs recorded in
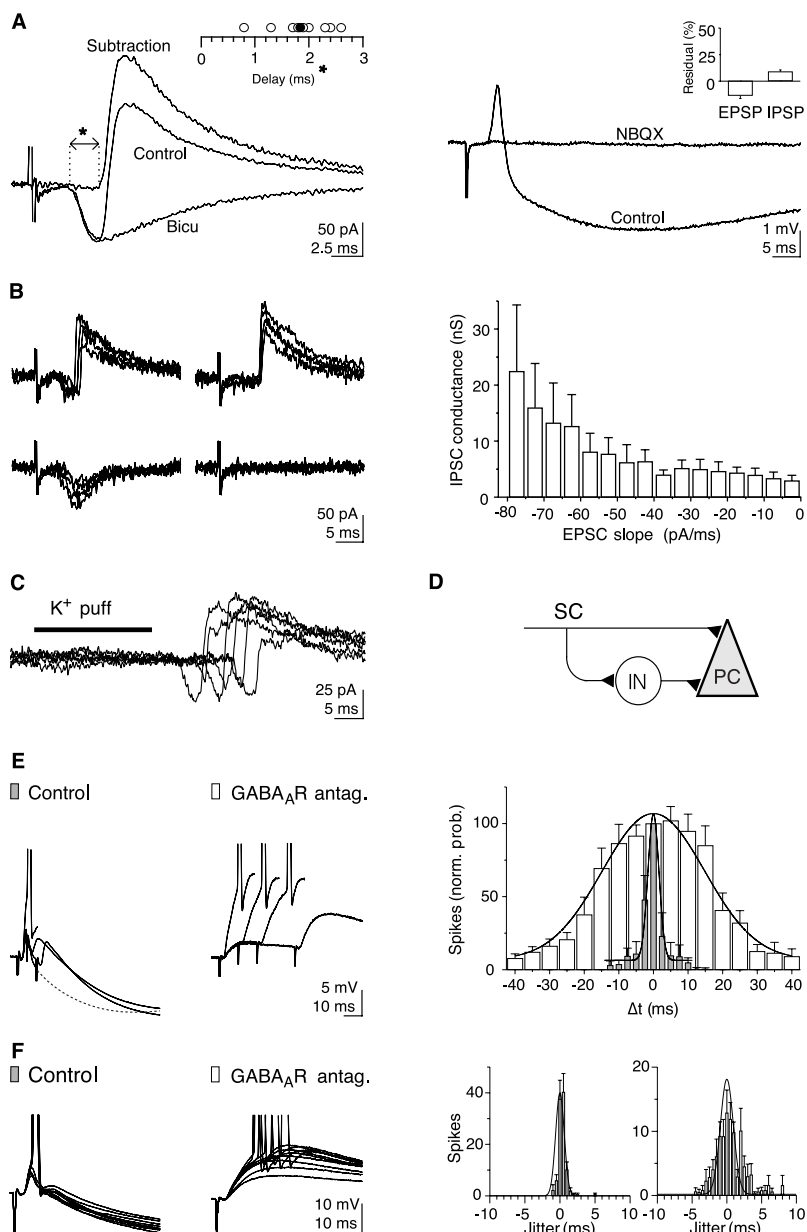
the dendrites occurs over a broader window (from –8.6 to +12.3 ms) (25). This difference was due to a preferential inhibitory input on the soma, first, because in bicuculline the window of EPSP summation was indistinguishable between both compartments (>60 ms; the average distance between pipettes was 200 ± 12 μm, and the range was from 168 to 236 μm; $n = 4$ cells; Fig. 4B). Second, imposing a somatic inhibitory conductance in the presence of SR95531 mimicked the somatic and dendritic integration windows observed under control conditions (soma, +1.8 ms; dendrite, +12.5 ms; the average distance between pipettes was 184 ± 20 μm, and the range was from 143 to 248 μm; $n = 4$ cells; Fig. 4C) (26).

Our data indicate that feed-forward inhibition limits temporal summation of EPSPs far below the mean interspike interval of PCs

(27), thus making them precise coincidence detectors (28). The presence of feed-forward inhibition in several major projections in the central nervous system (29) may thus serve as a means to maintain timing across brain areas (30).

The recruitment of GABAergic interneurons whose terminals preferentially impinge on or close to the soma rather than the apical dendrites leads these two compartments to integrate EPSPs over different time windows. Thus, summation of EPSPs to reach the threshold for action potential generation has to occur within less than 2 ms in CA1 PCs, whereas dendritic summation of the same EPSPs can occur over longer time periods. Cooperativity between separate inputs over long time windows may enable the expression of slower, voltage-dependent signaling [e.g., through *N*-

Fig. 2. Feed-forward inhibition is responsible for coincidence detection. (**A**) Whole-cell recordings from CA1 PCs upon Schaffer collateral stimulation. (Left panel) Current traces recorded in control conditions and bicuculline (bicu) and their algebraic difference (holding potential, –73 mV). (Left inset) Delays between the onset of the EPSC and the IPSC (the solid circle represents the average; $n = 9$ cells). (Right panel) Different cell, from the one on the left. The voltage traces recorded in control conditions and in NBQX are shown. The membrane potential is –66 mV. (Right inset) The residual EPSP and IPSP (% of control) in NBQX [$n = 12$ (six cells, 12 pathways)]. (**B**) (Left) Responses to low-intensity stimulation of Schaffer collaterals from a CA1 PC voltage clamped at –68 mV. Illustrated sweeps were collected with the same stimulation intensity and were ordered according to whether the stimulus evoked an EPSC-IPSC sequence, the failure of either component, or the complete failure of transmission. (Right) IPSC conductance is plotted against EPSC slope ($n = 14$ cells; bin width, 5 pA/ms). In all experiments, the stimulation intensity was slowly decreased until the complete failure of transmission occurred. (**C**) EPSC-IPSC sequences recorded in a CA1 PC voltage clamped at –58 mV and evoked by applying brief potassium puffs (1M KCl for 10 to 40 ms at 0.1 Hz) with a patch pipette on the CA3 cell body layer. (**D**) Schematic diagram of disynaptic feed-forward inhibition. SC, Schaffer collateral; IN, interneuron; PC, pyramidal cell. (**E**) Voltage traces for current-clamp recordings from CA1 PCs upon stimulation of two Schaffer collateral pathways. (Left) Control conditions; the dotted line is the average response to stimulation of one pathway. Continuous lines represent single responses to three different ISIs. (Middle) Four superimposed responses to four ISIs in bicuculline. Spikes were truncated. (Right) Histogram showing normalized probability of spike generation plotted against the ISI ($n = 8$ cells). Bin width in control, 2.5 ms for ISIs between ± 15 ms; 5 ms for longer ISIs (solid columns); bin width in GABA$_A$R antagonists, 5 ms (open columns). (**F**) The same cell as in (E), showing simultaneous stimulation of both pathways without (left) and with (middle) bicuculline. (Right) Histograms ($n = 8$ cells; bin width, 500 μs).

Fig. 3. Feed-forward inhibitory inputs selectively impinge on the soma of PCs. Drawing at top shows the recording configuration. (**A**) Voltage traces showing somatic (s, black) and dendritic (d, blue) responses to Schaffer collateral stimulation, in control conditions (left) and in bicuculline (middle). (Right) Summary graph showing dendritic EPSP amplitudes plotted against somatic EPSP amplitudes in control conditions (solid symbols) and in bicuculline (open symbols). Different symbols are shown for different experiments [$n = 10$ (9 cells, 10 pathways); the average distance between pipettes was 211 ± 19 μm; $n = 9$ cells]. (**B**) Same cell as in (A). Voltage traces; somatic (left) and dendritic (middle) recordings with and without bicuculline and their algebraic difference. (Right) Summary graph in which the integral of the algebraic difference between traces recorded in the presence and absence of bicuculline in the dendrites is divided by the corresponding integral in the soma and plotted against the distance between the two recording sites ($n = 9$ cells). (**C**) Different cell from that in (B). Voltage traces; somatic (s, black) and dendritic (d, blue) responses to Schaffer collateral stimulation in SR95531, without (left) and with (middle) dynamic current injection (lower trace) through the somatic pipette. (Right) Summary graph showing dendritic EPSP amplitudes plotted against somatic EPSP amplitudes under control conditions (open symbols) and with dynamic current injection (solid symbols). Different symbols are shown for different experiments (the average distance between pipettes was 200 ± 14 μm; $n = 9$ cells). (**D**) Same cell as in (C). Voltage traces showing somatic (left) and dendritic (middle) recordings in the presence and absence of dynamic current injection and their algebraic difference. (Right) Summary graph showing the ratio between the dendritic and somatic integrals of the algebraic differences between traces recorded in the presence and absence of dynamic current injection plotted against the distance between the two recording sites (solid symbols; $n = 9$ cells). Note the close match (apart from one experiment) with the data points obtained with the physiological activation of feed-forward inhibition [open symbols, taken from (B)].
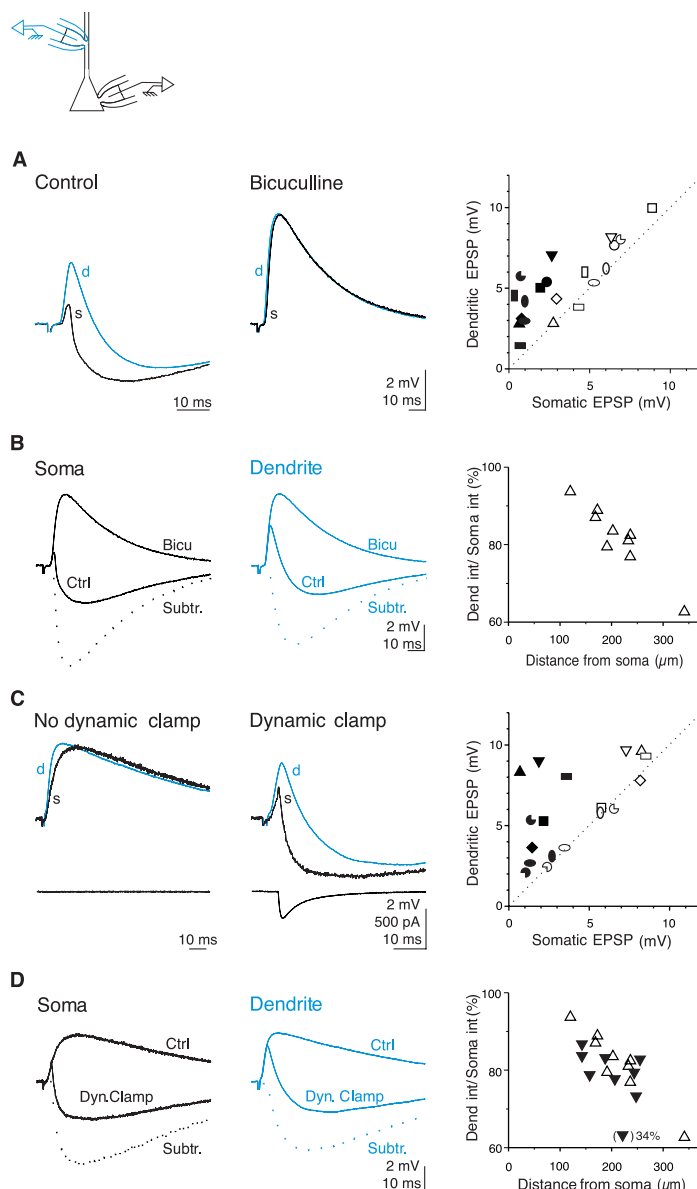
methyl-D-aspartate (NMDA) receptors], as may be necessary for the induction of lasting changes in synaptic strength.

Although interneurons innervating PC dendrites also receive excitatory inputs from Schaffer collaterals, providing the anatomical basis for dendritic feed-forward inhibition (*31*), their mode of activation remains to be clarified.

Noradrenaline and acetycholine can selectively regulate the excitability of subsets of GABAergic interneurons (*32*, *33*) and are released during different behavioral states (*34*, *35*). The excitability of interneurons will determine the delay and size of feed-forward inhibition and hence the size of the integration window. It is conceivable that according to the behavioral state of the animal, the operation mode of PCs shifts from precise coincidence detection to integration over large time windows.

References and Notes
1. S. Zhang, L. O. Trussel, *J. Neurophysiol.* **72**, 705 (1994).
2. N. Otmakhov, A. M. Shirke, R. Malinow, *Neuron* **10**, 1101 (1993).
3. G. Major, A. U. Larkman, P. Jonas, B. Sakmann, J. J. Jack, *J. Neurosci.* **14**, 4613 (1994).
4. M. Abeles, *Isr. J. Med. Sci.* **18**, 83 (1982).
5. W. R. Softky, C. Koch, *J. Neurosci.* **13**, 334 (1993).
6. M. N. Shadlen, W. T. Newsome, *Curr. Opin. Neurobiol.* **4**, 569 (1995).
7. Hippocampal slices (400 μm) were prepared from 30-day-old Wistar rats and incubated for 1 hour in an interface chamber at 35°C in artificial cerebrospinal fluid (ACSF) equilibrated with 95% O_2 and 5% CO_2, containing 119 mM NaCl, 2.5 mM KCl, 1.3 mM NaHPO$_4$, 1.3 mM MgCl$_2$, 2.5 mM CaCl$_2$, 26 mM NaHCO$_3$, and 11 mM glucose. The slices were kept at room temperature for 0 to 5 hours before being placed in a submerged chamber for recordings at 33°C, and the CaCl$_2$ concentration in the ACSF was increased by 2 mM. Unless stated otherwise, a cut was performed between the CA3 and CA1 regions. Cell-attached and whole-cell recordings of CA1 PCs, visually identified with infrared videomicroscopy, were performed with patch pipettes (3 to 10 megohms resistance for somatic recordings and 13 to 27 megohms resistance for dendritic and cell-attached recordings) filled with a solution containing 150 mM K gluconate, 5 mM Hepes, 1.1 mM EGTA, 0.5 to 1 mM MgCl$_2$, and 10 mM phosphocreatine, with the pH adjusted to 7.2 with gluconic acid. During voltage-clamp recordings, series resistance (7 to 10 megohms) was compensated by 60 to 70%. Steel electrodes were used for stimulation (100 μs; 5 to 205 μA). All experiments were performed in the presence of the GABA$_B$ receptor antagonist CGP62349 (1 μM) and the NMDA receptor antagonist 3-[(R)-2-Canboxypiperazin-4-yl]-propyl-1-phosphonic acid (D-CPP) (25 μM). Voltage measurements were corrected for the experimentally determined junction potential (13 mV). Average values are expressed as means $\pm$ SEM. The Student t test was used for statistical comparisons. Data were recorded with Axopatch 200 B and Axoclamp 2B amplifiers, digitized at 5 to 10 kHz, and analyzed offline. Drugs used were NBQX, 6-cyano-7-nitroquinoxaline-2,3-dione (CNQX), D-CPP, CGP62349, bicuculline, and SR95531. CGP62349 and D-CPP were a gift from Novartis (Basel, Switzerland).
8. V. Seutin, J. Scuvee-Moreau, A. Dresse, *Neuropharmacology* **36**, 1653 (1997).
9. Z. F. Mainen, T. J. Sejnowski, *Science* **268**, 1503 (1995).
10. At an average membrane potential of -69.2 ± 1.1 mV ($n = 5$ cells), the peak of the EPSP occurred 3 ± 0.1 ms
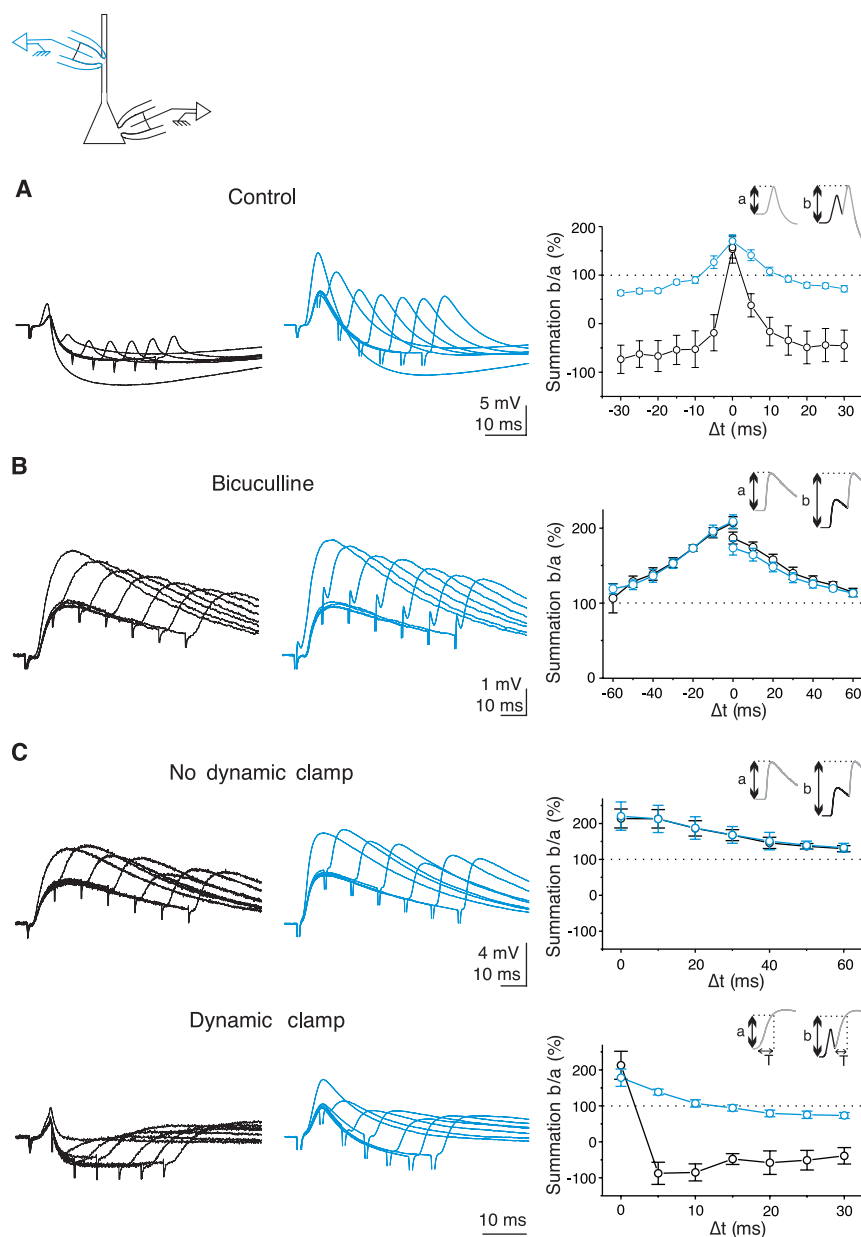
Fig. 4. Dendrites effectively summate EPSPs over broader time windows compared with the soma. Simultaneous somatic (black) and dendritic (blue) recordings from CA1 PCs upon stimulation of two Schaffer collateral pathways. The drawing at the top is as in Fig. 3. (**A**) Voltage traces showing seven superimposed somatic (left) and dendritic (middle) responses to seven different ISIs in control conditions. (Right) Summary graph showing the ratio of *b* to *a* plotted against the ISI, where *a* is the amplitude of the EPSP evoked by the stimulation of one pathway alone, and *b* is the maximal positive deviation from the resting membrane potential upon stimulation of that same pathway when preceded by the stimulation of the other pathway. Black symbols represent somatic recordings; blue symbols represent dendritic recordings (the average distance between pipettes was 229 ± 30 μm; $n = 6$ cells). (**B**) A different cell from that in (A). Conditions were as in (A), but in the presence of bicuculline (the average distance between pipettes was 200 ± 12 μm; $n = 4$ cells). (**C**) (Upper panels) Voltage traces showing seven superimposed somatic (left) and dendritic (middle) responses to seven different ISIs in the presence of SR95531. (Right) Summary graph ($n = 4$ cells). (Lower panels) Voltage traces showing the same cell with dynamic current injection in the soma (left and middle). (Right) Summary graph ($n = 4$ cells; the average distance between pipettes was 184 ± 20 μm).

after its onset, thus 1 ms later than the onset of the IPSC. Thus, although it contained both excitatory and inhibitory conductances we will refer to it as the peak of the EPSP.

11. The ratio of the IPSP slope in NBQX to the initial IPSP slope in control conditions. The dynamic clamp of an IPSC in the presence of GABA$_A$R antagonists (*23*) with or without Schaffer collateral stimulation indicates that such measurement overestimates the nor-malized residual IPSP by $19 \pm 4\%$ [$n = 11$ (nine cells, 11 pathways)].

12. The IPSC conductance was estimated by dividing the peak IPSC amplitude by the difference between the holding potential and the reversal potential of the IPSC.

13. For these experiments, we did not cut between the CA3 and CA1 regions. The puff pipette was moved along the CA3 PC layer until reproducible EPSC-IPSC sequences could be recorded.

14. W. D. Knowles, P. A. Schwartzkroin, *J. Neurosci.* **1**, 318 (1981).
15. R. Miles, R. K. Wong, *J. Physiol.* **356**, 97 (1984).
16. D. Debanne, N. C. Guerineau, B. H. Gähwiler, S. M. Thompson, *J. Neurophysiol.* **73**, 1282 (1995).
17. The EPSP slope evoked with simultaneous stimulation was $91 \pm 2\%$ of the algebraic sum of the EPSP slopes evoked by stimulation of each pathway separately, indicating pathway independence; $n = 7$ cells.
18. D. Jaeger, J. M. Bower, *J. Neurosci.* **19**, 6090 (1999).
19. T. F. Freund, G. Buzsaki, *Hippocampus* **6**, 347 (1996).
20. G. J. Stuart, H. U. Dodt, B. Sakmann, *Pfluegers Arch. Eur. J. Physiol.* **423**, 511 (1993).
21. The area was computed by subtracting the voltage traces in bicuculline from the traces in control conditions and integrating the resulting sweep over time.
22. This was not due to an increased driving force of the IPSP in the soma versus the dendrites because, as mentioned in the text, the amplitude of the EPSP in bicuculline was slightly larger in the dendrites and the half decay of EPSPs was not significantly different between compartments.
23. The conductance had the time course of a mono-synaptic IPSC evoked with an extracellular stimulation electrode in the presence of NBQX (20 μM) and CPP (25 μM) (τ_{rise}, 0.6 ms; τ_{decay1}, 3.9 ms; τ_{decay2}, 14 ms; the ratio of the amplitudes of the two components of decay was 63:37; $n = 4$ cells) and a peak amplitude within the experimentally observed range (13 to 25 nS; Fig. 2B). The amplitude of the injected current at any time point was equal to the conductance times the difference between membrane potential and the experimentally determined reversal potential of the IPSC. The operation was performed with an analog circuit (5-MHz bandwidth) connected to the amplifier. Input and output signals were filtered at 5 kHz. We computed the simulated IPSP-sensitive area by subtracting voltage traces in the absence of a simulated IPSP from traces in the presence of a simulated IPSP, and we integrated the resulting sweep over time.
24. The attenuation was compared between all dynamic clamp experiments ($n = 9$ cells) and those feed-forward IPSP experiments where the distances of the dendritic recording from the soma fell within the same range as with dynamic clamp experiments (the average distance was 206 ± 10 μm, and the range was from 169 to 237 μm; $n = 7$ cells).
25. Experiments that showed less than 85% IPSP reduction after NBQX perfusion were not considered. The integration window was given by the crossing of the line connecting the data points with the 100% line (Fig. 4).
26. For technical reasons, the IPSP could be simulated after the first stimulus only, and consequently the integration window was calculated only for positive delays. For consistency, the amplitude of the second EPSP was, nevertheless, measured at a time (*T*) on its rising phase equal to the time to peak of the EPSP of the first pathway.
27. J. O'Keefe, M. L. Recce, *Hippocampus* **3**, 317 (1993).
28. P. König, A. K. Engel, W. Singer, *Trends. Neurosci.* **19**, 130 (1996).
29. G. M. Shepherd, *The Synaptic Organization of the Brain* (Oxford Univ. Press, New York, ed. 4, 1998).
30. A. K. Sturm, P. König, *Biol. Cybern.* **84**, 153 (2001).
31. A. I. Gulyás, M. Megías, Z. Emri, T. F. Freund, *J. Neurosci.* **19**, 10082 (1999).
32. D. E. Bergles, V. A. Doze, D. V. Madison, S. J. Smith, *J. Neurosci.* **16**, 572 (1996).
33. A. R. McQuiston, D. V. Madison, *J. Neurosci.* **19**, 5693 (1999).
34. G. Aston-Jones, F. E. Bloom, *J. Neurosci.* **1**, 887 (1981).
35. H. Teitelbaum, J. F. Lee, J. N. Johannessen, *Science* **188**, 1114 (1975).
36. We are grateful to N. Arnth-Jensen, M. Carandini, B. H. Gähwiler, U. Gerber, and P. König for comments on the manuscript and to R. Kägi and H.-J. Kasper for technical assistance. Supported by the Swiss National Science Foundation.

23 February 2001; accepted 6 June 2001